Role of Cloud Feedback in Continental Warming Response to CO_2 Physiological Forcing

SO-WON PARK,[a] JONG-SEONG KUG,[a,b] SANG-YOON JUN,[c] SU-JONG JEONG,[d,e] AND JIN-SOO KIM[f]

[a] *Division of Environmental Science and Engineering, Pohang University of Science and Technology (POSTECH), Pohang, South Korea*
[b] *Institute for Convergence Research and Education in Advanced Technology, Yonsei University, Seoul, South Korea*
[c] *Korea Polar Research Institute, Incheon, South Korea*
[d] *Department of Environmental Planning, Graduate School of Environmental Studies, Seoul National University, Seoul, South Korea*
[e] *Institute for Sustainable Development (ISD), Seoul National University, Seoul, South Korea*
[f] *Department of Evolutionary Biology and Environmental Studies, University of Zurich, Zurich, Switzerland*

(Manuscript received 11 January 2021, in final form 23 June 2021)

ABSTRACT: Stomatal closure is a major physiological response to the increasing atmospheric carbon dioxide (CO_2), which can lead to surface warming by regulating surface energy fluxes—a phenomenon known as CO_2 physiological forcing. The magnitude of land surface warming caused by physiological forcing is substantial and varies across models. Here we assess the continental warming response to CO_2 physiological forcing and quantify the resultant climate feedback using carbon–climate simulations from phases 5 and 6 of the Coupled Model Intercomparison Project, with a focus on identifying the cause of intermodel spread. It is demonstrated that the continental (40°–70°N) warming response to the physiological forcing in summer (~0.55 K) is amplified primarily due to cloud feedback (~1.05 K), whereas the other climate feedbacks, ranging from −0.57 to 0.20 K, show relatively minor contributions. In addition, the strength of cloud feedback varies considerably across models, which plays a primary role in leading large diversity of the continental warming response to the physiological forcing.

KEYWORDS: Atmosphere-land interaction; Feedback; Climate models; Model comparison; Model evaluation/performance

1. Introduction

An increase in atmospheric carbon dioxide (CO_2) influences the climate system through not only its greenhouse radiative effect (CO_2 radiative forcing) but also its impact on plant physiology (CO_2 physiological forcing). Plants respond to elevated CO_2 levels by regulating their stomata (pores on the leaves, which simultaneously gain CO_2 and lose water) and increasing their photosynthetic rates. Stomatal apertures open less widely under elevated CO_2 levels to minimize water loss, thus reducing transpiration and increasing water use efficiency (rate of carbon uptake per unit of water lost) (Drake et al. 1997; Medlyn et al. 2001; Lammertsma et al. 2011; Keenan et al. 2013). This partial closure of the stomata affects the surface energy partitioning and thus increases boundary layer temperatures (CO_2 physiological forcing) (Betts et al. 2004; Long et al. 2006; Cao et al. 2010; Fatichi et al. 2016). At the same time, increasing CO_2 concentrations stimulate higher rates of photosynthesis (CO_2 fertilization effect) (Gunderson and Wullschleger 1994; Drake et al. 1997; Ainsworth and Long 2005). This effect contributes to a positive trend in the canopy leaf area (Zhu et al. 2016) and the terrestrial carbon sink (Schimel et al. 2015) and can increase plant transpiration, resulting in a cooling effect (Zeng et al. 2017). While the magnitudes of stomatal conductance response and fertilization effects vary depending on the plant type and environmental conditions such as water, light, and nutrient availability, both plant physiological responses can affect the climate system in opposite ways by altering the water and surface energy fluxes (Kergoat et al. 2002; Ainsworth and Long 2005; Cao et al. 2010; Donohue et al. 2013; Fatichi et al. 2016; Skinner et al. 2018).

Sellers et al. (1996) quantified the global-scale land surface warming caused by the stomatal response to increasing CO_2 from a coupled biosphere–atmosphere model for the first time. Betts et al. (1997) found that a change in the vegetation structure, an increase in the leaf area index (LAI), partially offsets the continental warming caused by stomatal closure. Since then, climate change forced by plant response to CO_2 has been quantified by using Earth system models (ESMs), which can simulate interactions between the physical climate system and biogeochemical processes, including the dependency of stomatal conductance and photosynthetic rates on CO_2. Continental warming driven by physiological effects constitutes 1.4%–13.9% of the warming caused by the combined effect of radiative and physiological forcing at a doubling of CO_2 ($2 \times CO_2$) (Zarakas et al. 2020). Especially in summer, the magnitude of physiologically driven continental warming in the boreal region (40°–70°N) accounts for 27.7% of the warming resulting from radiative forcing at average CO_2 concentrations of ~823 ppm (Park et al. 2020).

Multiple modeling studies consistently show that the stomatal effect increases the near-surface air temperature, overwhelming the evaporative cooling effect from the CO_2 fertilization

Supplemental information related to this paper is available at the Journals Online website: https://doi.org/10.1175/JCLI-D-21-0025.s1.

Corresponding author: Jong-Seong Kug, jskug@postech.ac.kr

DOI: 10.1175/JCLI-D-21-0025.1

(Cox et al. 1999; Boucher et al. 2009; Swann et al. 2016; Skinner et al. 2018; Lemordant et al. 2018; Hong et al. 2019). The CO_2 physiological effect limits evapotranspiration (ET) and enhances the ratio of sensible to latent heat fluxes at the leaf surface, thereby increasing boundary layer temperature. In addition, a decrease in cloud fraction caused by a physiologically driven reduction in relative humidity (RH) amplifies land surface warming by causing higher amounts of solar radiation to reach the surface (Doutriaux-Boucher et al. 2009; Andrews et al. 2011, 2012; de Arellano et al. 2012; Lemordant et al. 2018). Moreover, an increase in the LAI or expansion of forests generally decreases albedo, thereby additionally contributing to warming (Betts 2000; Bala et al. 2006; Pearson et al. 2013).

Most studies based on ESMs show that these physiological effects are a nonnegligible contributor to total-CO_2-forced land surface warming on a global scale, showing the robustness of the change of direction across models (Sellers et al. 1996; Cao et al. 2010; Park et al. 2020; Zarakas et al. 2020). However, the magnitude and spatial pattern of the surface warming substantially vary across these models; this variability significantly impacts the models' climate sensitivity (Joshi et al. 2008; Boucher et al. 2009; Geoffroy et al. 2012) and increases uncertainties in climate change projection. Zarakas et al. (2020) stated that intermodel disagreements about physiological-forcing-driven warming contribute to uncertainties in total-CO_2-forced warming. In some highly forested land regions, an intermodel disagreement in local surface warming at $2 \times CO_2$ is driven by approximately equal contributions of uncertainty from physiologically and radiatively forced warming. To reduce models' uncertainties in the projection of future climate warming, it is important to understand the intermodel spread in surface warming resulting from not only radiative forcing but also physiological forcing. However, the source of intermodel diversity in physiologically driven surface warming has yet to be assessed systematically despite its nonnegligible contribution to CO_2-forced climate warming.

Climate models exhibit a wide range of global mean surface temperature responses to increased radiative perturbation due to differences in feedback processes that amplify or dampen the initial radiative forcing (Cubasch and Cess 1990). In the classical radiative forcing–feedback framework, the radiative forcing is defined as an initial perturbation of top-of-atmosphere (TOA) radiation occurring in response to increasing CO_2. The radiative feedback is defined by a change in the net TOA radiation from a given change in feedback variables provoked by the initial radiative forcing (Hansen et al. 1984; Roe 2009). This forcing–feedback framework has helped establish the dominant role of water vapor feedback in amplifying global warming and has also identified the differences in cloud feedback as major sources of variations in the climate sensitivity of models (Cess 1990; Colman 2003; Soden and Held 2006; Bony et al. 2006). In addition, the quantification of local climate feedback has provided an opportunity to identify the processes responsible for local surface warming (e.g., Arctic warming) and its intermodel spread, thereby improving the understanding of regional climate change (Armour et al. 2013; Pithan and Mauritsen 2014; Goosse et al. 2018; Hwang et al. 2018).

It has been suggested that the radiation change due to physiologically driven changes in albedo, cloud cover, and column water vapor can be a mechanism for amplifying the land surface warming (Doutriaux-Boucher et al. 2009; Cao et al. 2010; Andrews et al. 2011; de Arellano et al. 2012; Lemordant et al. 2018). Park et al. (2020) suggested that continental warming over mid-to-high latitudes resulting from physiological forcing is enhanced by local feedback processes, such as cloud feedback and snow– and vegetation–albedo feedback. Moreover, it is also reported that the differences in climate feedback magnitude may cause intermodel spread in continental warming. However, such climate feedback triggered by physiological forcing has not been estimated quantitatively. Estimating the magnitude of climate feedback would help identify the main process responsible for temperature change and facilitate understanding of the diverse temperature responses across ESMs to physiological forcing, as in radiative forcing.

This study aims to quantitatively estimate the magnitude of local climate feedback triggered by physiological forcing, to identify the source of intermodel diversity in physiological-forcing-driven land surface warming, thereby providing better insights into the climate response to CO_2 physiological forcing. The rest of this paper is organized as follows. Section 2 describes the Coupled Model Intercomparison Project (CMIP) phase 5 and 6 datasets, the experimental design, and the method for quantifying climate feedback. In section 3, we first evaluate physiologically driven land surface warming and its intermodel spread across ESMs. Next, we estimate the contribution of climate feedback to continental warming and explain the primary cause of the intermodel spread in a CO_2 physiological forcing experiment. Finally, a summary and discussion are provided in section 4.

2. Data and methods

a. CMIP data and experimental design

We analyzed the idealized carbon–climate feedback experiments as part of the Coupled Climate–Carbon Cycle Model Intercomparison Project (C4MIP; Friedlingstein et al. 2006; Jones et al. 2016) from the CMIP5 and CMIP6 archives (Taylor et al. 2012; Eyring et al. 2016) to evaluate the impacts of CO_2 physiological forcing on the climate and understand their intermodel spread. These experiments were designed to quantify the strength of interactions between the carbon cycle and the climate in state-of-the-art climate models. The experiments were run for 140 years with a CO_2 increase of 1% per year from preindustrial levels to a quadrupling for radiation and biogeochemistry (full), radiation only (radiation), and biogeochemistry only (physiology), while all other forcings remained at preindustrial levels. We used the preindustrial experiment as the baseline (control). The experiments used in this study are described in Table 1. For GFDL-ESM2M, the atmospheric CO_2 levels were prescribed to increase from their initial mixing ratio level of 286.15 ppmv at a rate of 1% per year until year 70 ($2 \times CO_2$); thereafter, CO_2 levels were kept constant for the remainder of the run.

To quantify the CO_2 physiological forcing (Phy) (average CO_2 concentrations ~820 ppm), we calculated the difference between the averages for years 71–140 of two simulations: the

TABLE 1. List of CMIP simulations used in this study.

Experiment	CMIP5 simulation	CMIP6 simulation	Description
Full	1pctCO2	1pctCO2	Both radiation and carbon cycle see 1% per year increase in atmospheric CO_2 for 140 years from preindustrial CO_2 concentration to quadrupling (from 285 to 1140 ppm)
Physiology	esmFixClim1	1pctCO2-bgc	Radiation code sees preindustrial CO_2 concentration, but carbon cycle sees 1% yr^{-1} CO_2 increase to quadrupling for 140 years (from 285 to 1140 ppm)
Radiation	esmFdbk1	1pctCO2-rad	Carbon cycle sees preindustrial CO_2 concentration, but radiation code sees 1% yr^{-1} CO_2 increase to quadrupling for 140 years (from 285 to 1140 ppm)
Control	piControl	piControl	Pre-industrial control run

physiology simulation (esmFixClim1 in CMIP5; 1pctCO2-bgc in CMIP6) and control simulation (piControl). When using the control simulation, we accounted for model drifts by subtracting the linear trend of the corresponding period, following previous studies (Gregory and Forster 2008; Zarakas et al. 2020). The physiological forcing can also be evaluated by computing the difference between the full CO_2 simulation (1pctCO2) and the radiation simulation (esmFdbk1 in CMIP5; 1pctCO2-rad in CMIP6). However, this includes nonlinear interactions between radiative forcing and physiological forcing (Bathiany et al. 2014; Skinner et al. 2017), thus complicating the interpretation. To avoid this complexity, we calculated anomalies of each forcing experiment using the control simulation (piControl) as the baseline. Similarly, we quantified the radiative forcing without nonlinear interactions by computing the difference between the averages for years 71–140 between the radiation simulation (esmFdbk1 in CMIP5; 1pctCO2-rad in CMIP6) and the control simulation (piControl) for the comparison with the physiological forcing.

We used 19 ESMs (8 CMIP5 models and 11 CMIP6 models) that performed carbon–climate feedback experiments and uploaded all variables needed for the analysis of the warming contributions from individual feedbacks to the Earth System Grid Federation (ESGF) repository by 20 May 2021 (Table 2). A multimodel ensemble (MME) was derived by regridding the outputs from the ESMs to a common $1° \times 1°$ grid and then averaging them. The bootstrap method was used to test the statistical significance of the difference between the experiments. For the MME, 19 values were randomly selected from the 19 ESMs with replacements, and their average was computed. This process was repeated 1000 times, the confidence intervals were determined, and only significant values were shown to indicate model agreement.

b. *Quantification of warming contribution from feedback factors*

The radiative imbalance at the TOA (ΔR; in W m^{-2}) in response to a forcing (F; in W m^{-2}) can be expressed as

$$\Delta R = F + \lambda \Delta T_s, \tag{1}$$

where λ is the net feedback parameter (W m^{-2} K^{-1}) and ΔT_s is the surface temperature change (K) (Gregory et al. 2004, 2015; Knutti and Hegerl 2008; Winton et al. 2010; Yoshimori et al. 2016). The total feedback parameter can be decomposed into individual feedback components as

$$\lambda = \lambda_T + \lambda_A + \lambda_W + \lambda_C, \tag{2}$$

where λ_T, λ_A, λ_w, and λ_C are the feedback parameters associated with the temperature, albedo, water vapor, and cloud, respectively. The temperature feedback can be further decomposed into contributions from vertically uniform warming of the surface and the troposphere (Planck feedback λ_P), and from tropospheric warming that deviates from the vertically uniform profile (lapse rate feedback λ_{LR}). In addition, the climate feedback parameters can be separated into shortwave (SW) and longwave (LW) components.

To assess the relative contributions of each feedback to the local surface warming, we used the extended radiative kernel technique, following previous studies (Pithan and Mauritsen 2014; Goosse et al. 2018), based on the local energy budget equation

$$F + \left(\lambda_P + \sum_i \lambda_i\right)\Delta T_s + \Delta\mathrm{AHT} + \Delta\mathrm{SHF} = 0, \tag{3}$$

where ΔAHT represents the change in atmospheric heat flux convergence (positive into the atmospheric column) and ΔSHF is the change in total energy flux from the surface (positive into the atmospheric column). When Eq. (3) was expanded from Eq. (1), the ΔR term was ignored due to its comparatively small magnitude. We can assess the temperature change associated with a particular feedback or forcing by dividing Eq. (3) by the magnitude of the global-mean Planck response $\overline{\lambda_P}$,

$$\begin{aligned}\Delta T_s = &-F/\overline{\lambda_P} - \lambda_p' \Delta T_s/\overline{\lambda_P} - \sum_i \lambda_i \Delta T_s/\overline{\lambda_P} \\ &- \Delta\mathrm{AHT}/\overline{\lambda_P} - \Delta\mathrm{SHF}/\overline{\lambda_P},\end{aligned} \tag{4}$$

where the terms on the right-hand side represent an individual warming contribution to the total local surface warming and λ_p'

TABLE 2. List of CMIP5 and CMIP6 ESMs (land surface models) used in this study. (Expansions of most acronyms are available online at http://www.ametsoc.org/PubsAcronymList.)

Modeling center (or group)	CMIP5	CMIP6	References
Beijing Climate Center, China Meteorological Administration	BCC-CSM1-1 (BCC-AVIM1.0)	BCC-CSM2-MR (BCC-AVIM2)	Wu et al. (2013), Wu et al. (2019)
Canadian Centre for Climate Modeling and Analysis	CanESM2 (CLASS2.7)	CanESM5 (CLASS3.6)	Arora et al. (2011), Swart et al. (2019)
National Center for Atmospheric Research	CESM1-BGC (CLM4)	CESM2 (CLM5)	Lindsay et al. (2014), Danabasoglu et al. (2020)
NOAA Geophysical Fluid Dynamics Laboratory	GFDL-ESM2M (LM3)		Dunne et al. (2012)
Met Office Hadley Centre	HadGEM2-ES (JULES)	UKESM1-0-LL (JULES-ES-1.0)	Jones et al. (2011), Sellar et al. (2019)
Institute Pierre Simon Laplace	IPSL-CM5A-LR (ORCHIDEE)	IPSL-CM6A-LR (ORCHIDEEv2.0)	Dufresne et al. (2013), Boucher et al. (2020)
Max Planck Institute for Meteorology	MPI-ESM-LR (JSBACH)	MPI-ESM-1-2-LR (JSBACH3.20)	Giorgetta et al. (2013), Mauritsen et al. (2019)
Norwegian Climate Centre	NorESM1-ME (CLM4)	NorESM2-LM (CLM5)	Tjiputra et al. (2013), Seland et al. (2020)
Commonwealth Scientific and Industrial Research Organization		ACCESS-ESM1-5 (CABLE2.4)	Ziehn et al. (2020)
Centro Euro-Mediterraneo sui Cambiamenti Climatici		CMCC-ESM2 (CLM4.5)	Cherchi et al. (2019)
Centre National de Recherches Météorologiques		CNRM-ESM2-1 (Surfex 8.0c)	Séférian et al. (2019)
Japan Agency for Marine-Earth Science and Technology		MIROC-ES2L (MATSIRO6.0)	Hajima et al. (2020)

represents the deviation of the local Planck response from its global-mean value. For example, the albedo feedback contribution to surface warming is the third term in Eq. (4) where λ_i is λ_A, and the atmospheric heat transport contribution to surface warming is the fourth term.

The local feedback parameters for each variable X were calculated through the radiative kernel method (Soden and Held 2006; Soden et al. 2008; Shell et al. 2008):

$$\lambda_X = \frac{dR}{dX_i}\frac{\Delta X_i}{\Delta T_s} = k_i \frac{\Delta X_i}{\Delta T_s}, \tag{5}$$

where k_i is the radiative kernel and X_i is the response of the climate variables to the changing surface temperature. The radiative kernel k_i is the change in TOA radiation caused by a change in the climate variable X_i and is derived using a specific radiative transfer code. Here, we used the radiative kernels created by Shell et al. (2008) using the Community Atmosphere Model version 3, from the National Center for Atmospheric Research. For the temperature feedback and water vapor feedback, only the troposphere was considered to exclude the stratospheric adjustment effect. To separate the tropospheric and stratospheric responses, we assumed a tropopause height of 100 hPa in the tropics (30°S–30°N) that decreases linearly with latitude to 300 hPa at the poles. Cloud feedback cannot be quantified directly from a radiative kernel due to its strong nonlinearity. However, it can be estimated from the change in cloud radiative forcing caused by the cloud response to the changes of various factors such as temperature and humidity provoked by CO_2 physiological forcing, and the variation of other climate feedbacks due to the cloud effect calculated from the difference of climate feedbacks between the all-sky and clear-sky conditions, as suggested in Soden et al. (2008). The change ΔSHF was diagnosed as the anomalous net surface heat fluxes, and ΔAHT was evaluated as the difference between ΔSHF, net TOA radiation flux anomaly, and heat storage in the atmosphere.

3. Results

a. *Continental warming resulting from CO_2 physiological forcing*

Prior to examining the climate feedback triggered by CO_2 physiological forcing, we evaluated the MME annual mean changes in the near-surface air temperature resulting from the physiological effect, which encompasses both stomatal and CO_2 fertilization effects. Physiological forcing causes significant land surface warming over the globe (MME mean: 0.38 K), especially in forested regions (Fig. 1). The magnitude of temperature change varies with latitude, with the greatest continental warming mainly in boreal forests (MME mean: 0.55 K), followed by the tropics. All ESMs except CNRM-ESM2-1 generally show similar spatial patterns of global temperature response and its latitudinal variation (Fig. 1 in the online supplemental material). On the basis of these results, our focus will be on the physiological effect in mid-to-high-latitude continents (40°–70°N), which show the greatest warming.

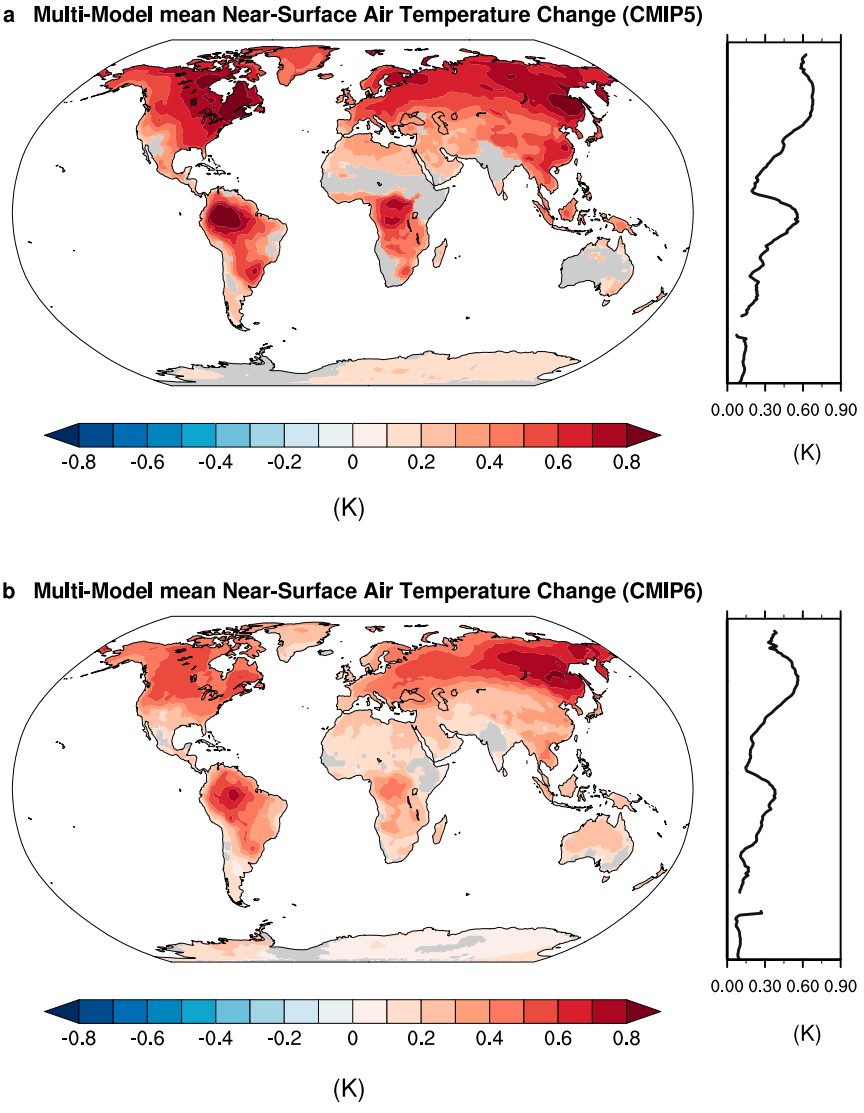

FIG. 1. Multimodel mean of annual mean changes in near-surface air temperature over the continents resulting from CO_2 physiological forcing in (a) CMIP5 and (b) CMIP6. The significant test is done based on the bootstrap method to test the model agreement. Insignificant values at the 95% confidence level are colored in gray. The zonal average of air temperature (only land grid points) is plotted on the right side of the map.

Next, we examine the seasonal changes in the near-surface air temperature caused by physiological effects over mid-to-high-latitude continents and the globe (Figs. 2a,b). The continental warming over 40°–70°N is the greatest in boreal summer [June–August (JJA)], when photosynthesis is most active, in accordance with plants' phenological cycle. The seasonal cycle of physiologically driven ET change is analogous to that of temperature change, demonstrating that the decreased ET can induce continental warming (Figs. 2c,d). On a global scale, seasonal changes in temperature and ET are similar to those in the mid-to-high latitudes, although global average anomalies are slightly smaller in magnitude. Considering this seasonality, we will focus on the physiological effect, especially in boreal summer, when the influence of CO_2 physiological forcing on temperature and ET is the strongest.

Meanwhile, the MME mean of physiological-forcing-driven temperature change has decreased in CMIP6 relative to CMIP5 in all seasons, although this difference is not statistically significant. This change is contrary to the tendency of CO_2 radiative forcing with the increased climate sensitivity in CMIP6 (Zelinka et al. 2020). We will further discuss the change from CMIP5 to CMIP6 and its cause in the summary and discussion section (section 4).

Most models consistently show a decreased ET and resultant land surface warming caused by physiological forcing (Fig. 3). However, the intermodel diversity of changes in ET

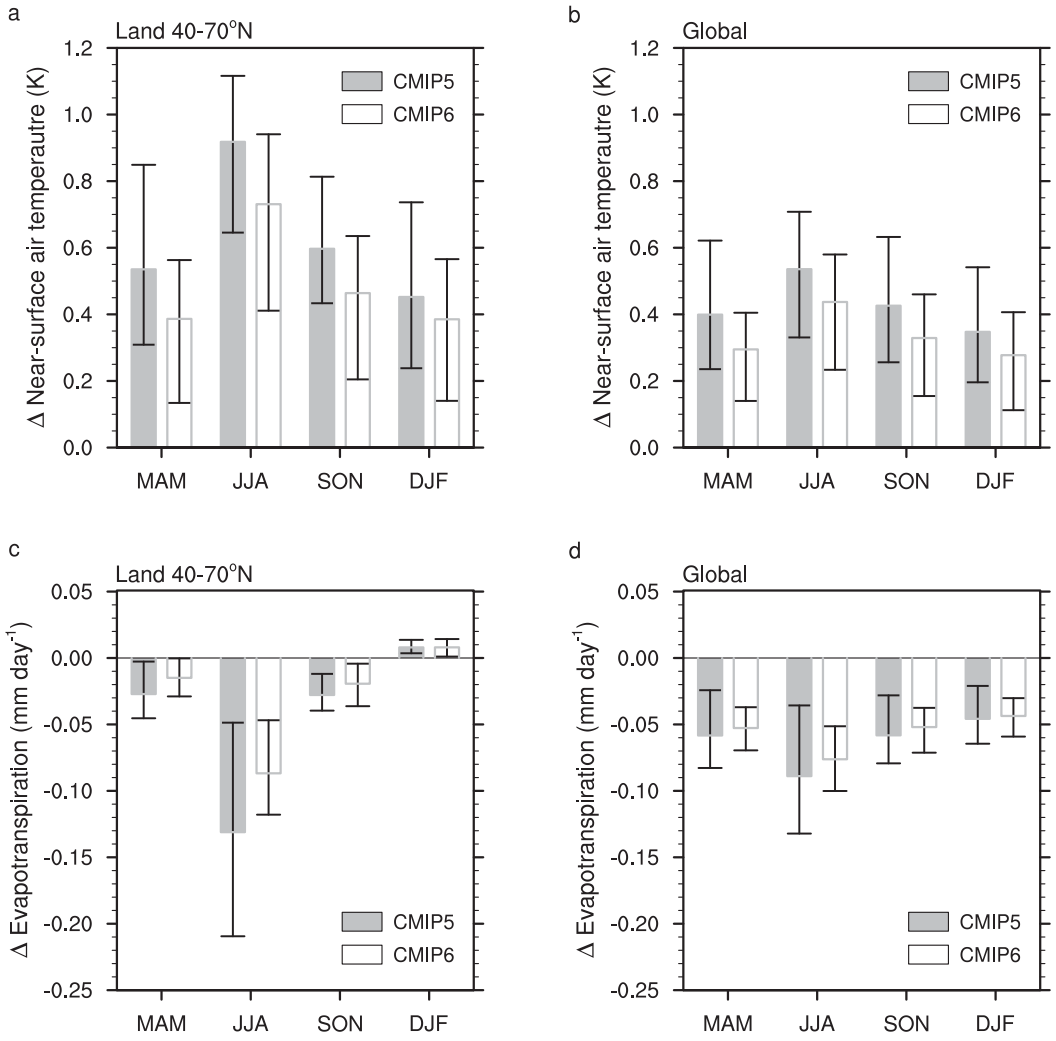

FIG. 2. Multimodel mean of seasonal changes in (a),(b) near-surface air temperature and (c),(d) ET resulting from CO_2 physiological effect averaged over (left) the mid-to-high-latitude continents (40°–70°N), and (right) global land areas excluding Antarctica. The gray bars show the MME mean from the 8 CMIP5 models, and the white bars show the MME mean from the 11 CMIP6 models. The error bars indicate the range of the 95% confidence level on the basis of the bootstrap method.

(range: from −0.36 to 0.02 mm day^{-1} in JJA) and resultant continental warming (range: from −0.25 to 1.82 K in JJA) is substantial, and this contributes to the uncertainty in total-CO_2-forced climate change. Since the decreased ET, a result of stomatal response to increasing CO_2, induces temperature rise through a repartition of surface turbulent fluxes, the change in ET can be regarded as a variable that directly represents the physiological effect on the climate system. The physiological influence on ET and temperature shows a significant negative correlation in JJA ($r = -0.66$, $P < 0.01$), but that correlation in the annual mean is weaker and not significant ($r = -0.4$, $P = 0.09$). This result suggests that the reduced ET driven by stomatal closure (initial perturbation) can explain the intermodel diversity of surface warming only to some extent, but not sufficient.

For example, even though the amount of change in ET, considered a representative variable of physiological forcing, is similar between models (ranging from 0 to −0.1 mm day^{-1}), the magnitude of surface warming is considerably different (Fig. 3). These results imply that climate feedback processes besides initial forcing might contribute to the diverse climate model sensitivities to CO_2 physiological forcing, as in the radiative forcing. Therefore, we attempted to identify the source of the intermodel spread in climate sensitivity to physiological forcing by quantifying the contributions of climate feedback to surface warming in the following section.

b. *Quantification of climate feedback triggered by CO_2 physiological forcing*

On the basis of the perspective of the traditional forcing–feedback framework (Gregory et al. 2004; Bony et al. 2006;

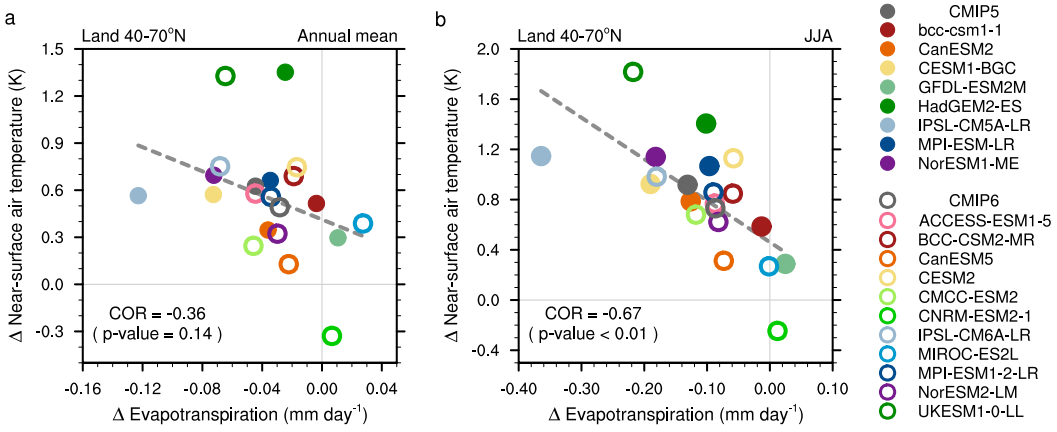

FIG. 3. (a) Scatterplot of annual mean changes in ET vs near-surface air temperature resulting from CO_2 physiological forcing averaged over the mid-to-high-latitude continents (40°–70°N). (b) As in (a), but for JJA. The gray dashed lines represent the least squares regression fits.

Roe 2009), plants' physiological responses to atmospheric CO_2 can be classified as part of forcing rather than the feedback because they respond quickly and directly to the CO_2 increase rather than to the temperature change (Zarakas et al. 2020). The modification of TOA radiative fluxes triggered by the initial perturbation, that is, physiologically driven surface warming, can be considered climate feedback. For example, the radiative imbalance due to the change of atmospheric water vapor caused by physiological-forcing-driven temperature rise could be classified as climate feedback.

Figure 4 shows the relationship between the total warming contribution—from individual feedback and atmospheric forcing—and temperature changes in the CO_2 physiological forcing experiment. To intuitively understand the role of feedback in surface warming, we quantified the temperature changes associated with each feedback based on Eq. (4), not the radiative flux changes, which are usually used for diagnosing the feedback. The annual mean anomalies are closely located along the 1:1 line, where models are expected to be if the total warming contribution from each feedback agrees with the temperature change; this finding confirms that feedback processes well explain the temperature change in models. Anomalies in JJA have some discrepancies due to inaccuracies in the feedback calculations but show a statistically significant positive correlation ($r = 0.95$, $P < 0.01$). Therefore, the application of the forcing–feedback framework to physiological forcing can help us understand the climate sensitivity in CO_2 physiological forcing experiment and its intermodel spread with some degree of accuracy.

We investigate which feedback processes are responsible for the continental warming in the radiative forcing and

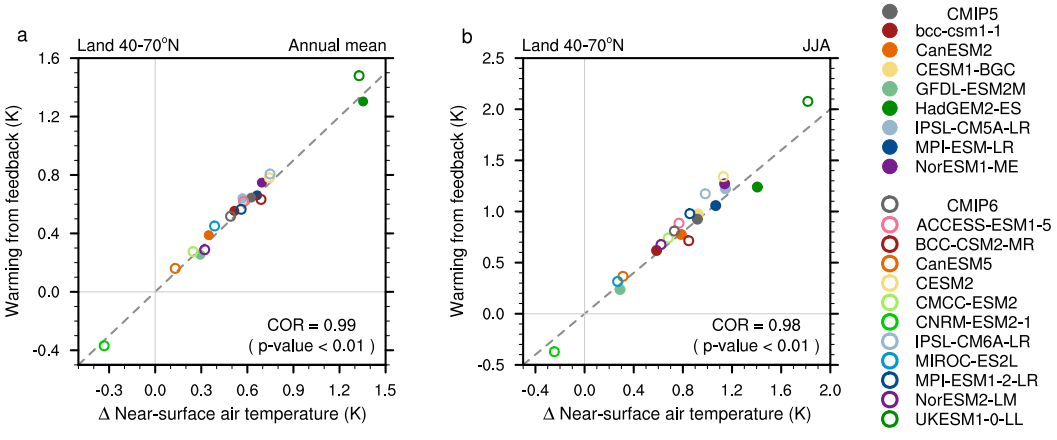

FIG. 4. (a) Scatterplot of annual mean changes in near-surface air temperature vs the sum of warming from forcing and individual feedback for the 8 CMIP5 models and 11 CMIP6 models in the CO_2 physiological forcing experiment. All values are weighted averages over the mid-to-high-latitude continents (40°–70°N). (b) As in (a), but for JJA. The gray 1:1 line is where the change in the near-surface air temperature is equal to the total warming from the forcing and individual feedback.

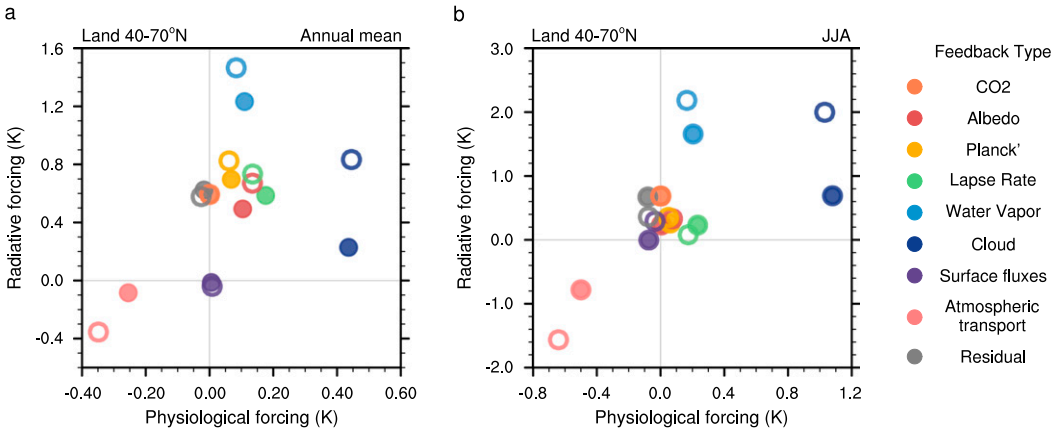

FIG. 5. (a) Scatterplot of annual mean continental (40°–70°N) warming contributions of forcing and individual feedback mechanisms resulting from CO_2 physiological forcing vs those resulting from CO_2 radiative forcing. (b) As in (a), but for JJA. Note the different scales in (a) and (b). The marker types indicate the CMIP phase (CMIP5: closed circle, CMIP6: open circle).

physiological forcing experiments. Figure 5 shows the continental warming contribution of the individual feedback caused by the radiative and physiological forcings based on a multimodel mean. In agreement with previous studies, we find that water vapor feedback is a major process that amplifies continental warming in the radiative forcing experiment (Colman 2003; Soden and Held 2006; Bony et al. 2006). In the radiative forcing, cloud feedback has relatively minor importance in annual land surface warming, although it is the second-largest positive feedback in boreal summer.

On the contrary, in the physiological forcing experiment, the cloud feedback overwhelmingly contributes to the land surface warming, and the other feedback processes play a minor role (Fig. 5 and supplemental Fig. 2; see also Table 3). Stomatal closure instantaneously reduces transpiration at the surface, thereby decreasing RH (Joshi et al. 2008). Additionally, turbulence thermals invigorated by the physiologically driven increase in sensible heat flux cause a deepening of the atmospheric boundary layer (ABL), provoking the entrainment of warm and dry air from the troposphere (Doutriaux-Boucher et al. 2009; de Arellano et al. 2012). Consequently, these conditions suppress clouds over land, and the reduced cloud fraction amplifies land surface warming by increasing downward SW radiation.

Following cloud feedback, lapse rate feedback is the greatest positive feedback, although it shows a considerable gap from cloud feedback. Positive lapse rate feedback occurs because the air near the surface is heated more than the air in the upper atmosphere due to the direct influence of plant physiological response (supplemental Fig. 3c). In addition, less latent heat release in the mid-to-upper troposphere due to reduced ET may intensify the bottom-heavy warming profile, contributing to the positive lapse rate feedback. The water vapor feedback as the third greatest positive feedback amplifies the surface warming. The air temperature rise considerably increases the amount of water vapor especially in the midtroposphere (supplemental Figs. 3b,c). As a result, the column water vapor generally increases (supplemental Fig. 3d), leading to the positive water vapor feedback. The albedo feedback is slightly positive possibly due to the changes in LAI and snow fraction caused by physiological forcing (supplemental Fig. 4).

The surface flux term, which reflects increased sensible heat and decreased latent heat fluxes triggered by stomatal closure, plays an almost neutral role in warming because these turbulent heat flux changes are balanced with surface radiative flux changes. The physiological forcing–induced warming is the greatest in the mid- to high latitudes and thus the atmospheric heat transport diverges, which plays a role in attenuating the surface warming, indicating negative feedback. This result is in good agreement with previous studies showing that the atmosphere transports energy away from regions of energy accumulation through the diffusive moist energy transport (Rose et al. 2014; Roe et al. 2015; Stuecker et al. 2018). Because of this energy transport, physiological forcing can drive the remote impacts on the ocean and Arctic region (Park et al. 2020; Zarakas et al. 2020).

TABLE 3. The MME mean of warming contributions from individual feedbacks resulting from CO_2 physiological forcing.

	Mid- to high-latitude continents (40°–70°N)		Global mean	
Feedback type (K)	ANN	JJA	ANN	JJA
Albedo	0.12	0.04	0.03	0.03
Local Planck	0.06	0.05	—	—
Lapse rate	0.15	0.20	0.01	0
Water vapor	0.09	0.18	0.08	0.10
Cloud	0.44	1.05	0.10	0.18
Surface fluxes	0	−0.05	−0.02	−0.04
Atmospheric heat transport	−0.31	−0.58	—	—

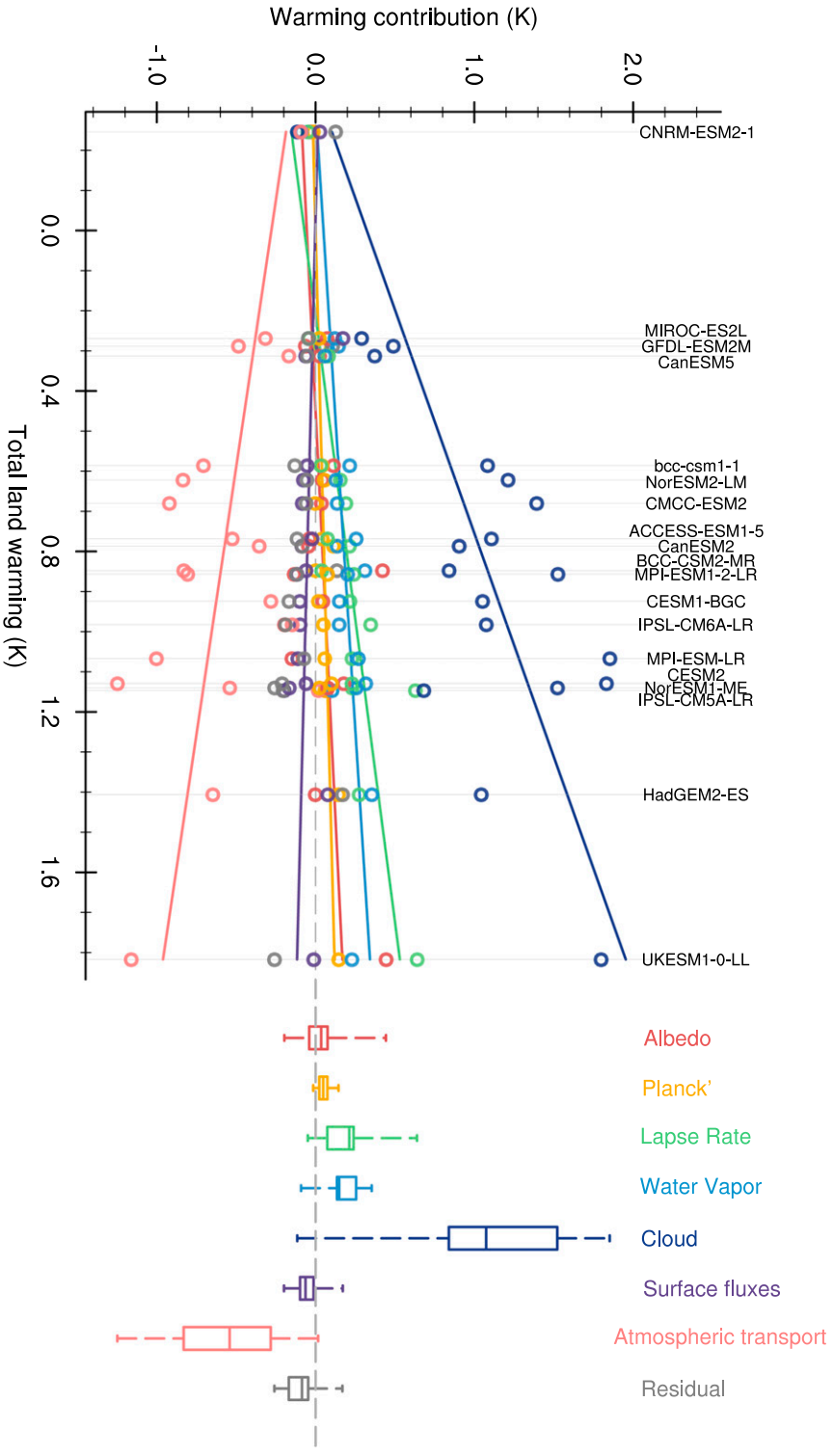

FIG. 6. Intermodel spread of continental (40°–70°N) warming contributions of individual feedback mechanisms by CO_2 physiological forcing in JJA. The colored lines represent the linear regressions of the warming contributions of the feedback processes against the total continental warming. The box plots show the median and the 25th and 75th percentiles of the continental warming contributions of the individual feedback mechanisms, and the whiskers show the full ensemble spread.

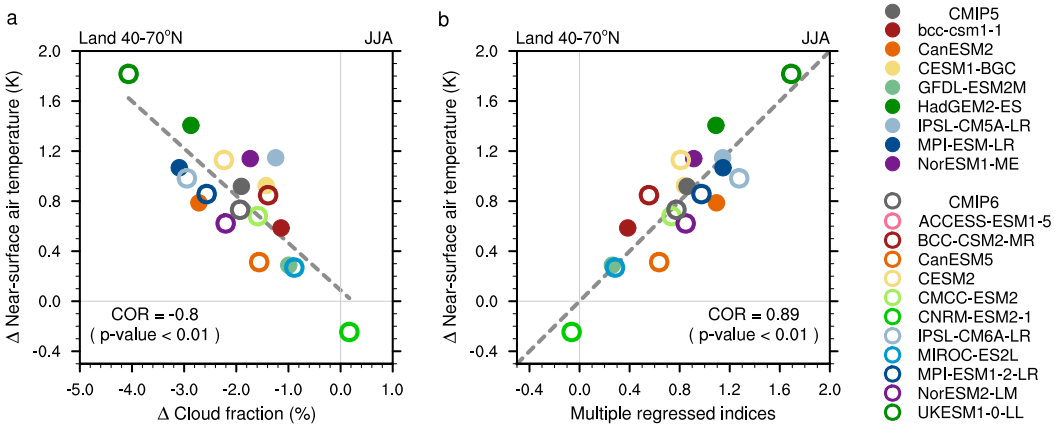

FIG. 7. (a) Scatterplot of changes in cloud fraction vs near-surface air temperature for JJA resulting from CO_2 physiological forcing averaged over the mid-to-high-latitude continents (40°–70°N). The gray straight dashed line represents the least squares regression fit. (b) Scatterplot of multiple regressed indices vs changes in temperature for JJA resulting from CO_2 physiological forcing averaged over the mid-to-high-latitude continents (40°–70°N). Multiple regressed indices are reconstructed by applying multiple linear regression to the air temperature with respect to standardized ET and cloud fraction as predictors. The gray 1:1 line is where the multiple regressed indices are equal to changes in air temperature resulting from CO_2 physiological forcing. Note that ACCESS-ESM1-5 does not provide cloud fraction data.

Besides quantifying the different feedback contributions to land surface warming in the ensemble mean, it is also important to understand why the degree of continental warming in physiological forcing varies across models. We found that the intermodel spread of continental warming in the physiological forcing experiment is largely dominated by the spread in local cloud feedback (Figs. 5 and 6). Changes in atmospheric heat transport dampen the intermodel diversity because they are more negative in ESMs with greater continental warming. Although the targeted region is different, this tendency is similar to that in previous studies reporting that warming and energy transport change are negatively correlated in the Arctic region (Hwang et al. 2011; Pithan and Mauritsen 2014). Lapse rate feedback and albedo feedback slightly contribute to the intermodel spread. In summary, the cloud feedback triggered by stomatal closure plays a key role in both the continental warming response to physiological forcing and its intermodel spread.

c. *Intermodel spread in cloud feedback*

Changes in ET alone cannot fully explain the diversity of surface warming responses to physiological forcing in ESMs, as the explained variance by ET is 44% ($r = -0.66$, $P < 0.01$) (Fig. 3b). As shown in Fig. 6, cloud feedback is the largest term in explaining the continental warming response to physiological forcing. Figure 7a shows the relation between cloud fraction and surface air temperature in an intermodel space. It is evident that a large cloud reduction is closely associated with a large temperature increase, emphasizing the importance of cloud feedback. The correlation between them is −0.84, which is significant at the 99% confidence level. We applied multiple linear regression to the temperature with respect to standardized ET and cloud fraction; results show that their combined effect can explain ~83% of the temperature change between ESMs ($r = 0.91$, $P < 0.01$) (Fig. 7b). By eliminating the correlation between ET and cloud, we also find that the ET alone can explain 17% of temperature variation across the ESMs and the cloud response to physiological forcing alone can explain the 44% of that, which demonstrates the importance of cloud feedback for understanding of intermodel diversity. Considering cloud feedback together with ET change could provide a better understanding of the intermodel diversity in the warming response to CO_2 physiological forcing. In this section, we will further examine the cause of the differences in magnitudes of cloud feedback between ESMs and their impact on temperature change.

Cloud feedback can be decomposed into SW and LW components (Fig. 8a). SW cloud feedback intensifies surface warming (MME mean: 1.15 K), whereas LW cloud feedback slightly dampens the temperature rise (MME mean: −0.1 K). This result confirms the hypothesis that cloud fraction reduction can contribute to the additional surface warming by enhancing the downward SW radiative flux. In terms of intermodel diversity, the spread in total cloud feedback mostly comes from SW rather than LW cloud feedback.

Even under similar reductions in ET, a trigger of cloud feedback, changes in cloud fraction might differ between models (supplemental Fig. 5). Thus, we identified the process that induces the intermodel diversity in cloud feedback among a series of processes—from stomata closure to cloud reduction (Figs. 8b–d). The ET and the Bowen ratio (sensible heat flux/latent heat flux) show a strong linear negative relationship ($r = -0.93$, $P < 0.01$). The correlation coefficient between the Bowen ratio and RH is also significant at the 95% confidence level ($r = -0.58$, $P = 0.02$), but it is relatively weakened because of the presence of three outlier ESMs (HadGEM2-ES, IPSL-CM5A-LR, and UKESM1-0-LL). These models also tend to act as outliers in the surface warming

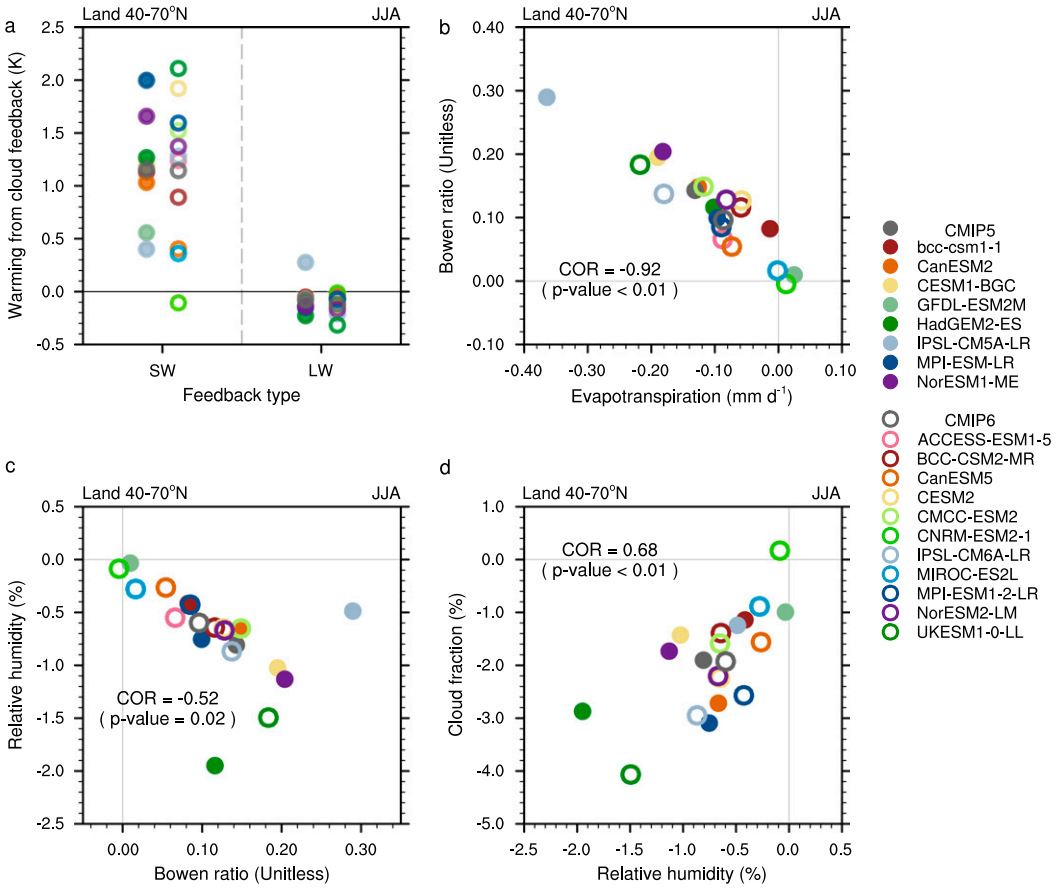

FIG. 8. (a) Breakdown of the warming contribution of cloud feedback into SW and LW components. Scatterplot of changes in (b) ET vs Bowen ratio (sensible heat flux/latent heat flux), (c) Bowen ratio vs RH, and (d) RH vs total cloud fraction in the CO_2 physiological forcing experiment. All values are weighted averages over the mid-to-high-latitude continents (40°–70°N) for JJA.

response to ET changes (Fig. 3). Furthermore, ESMs show a wide range of changes in cloud fraction even if changes in RH are almost the same (Fig. 8d).

To examine the model diversity further, we selected the five models with the greatest temperature responses (CMIP5: HadGEM2-ES and MPI-ESM-LR; CMIP6: BCC-CSM2-MR, CESM2, and MPI-ESM1-2-LR) and the five models with the weakest temperature anomalies (CMIP5: BCC-CSM1-1; CMIP6: ACCESS-ESM1-5, CanESM5, MIROC-ES2L, and NorESM2-LM) among 10 models with similar ET changes (from 0 to -0.11 mm day^{-1}), as shown in Fig. 3b, and then conducted a composite analysis (Fig. 9). In the top five models, RH and cloud fraction decrease more over a wider area than those in the bottom five models, and the top five models show a stronger continental warming response.

These results suggest that the diverse ET changes and physical processes, such as land–atmosphere coupling and cloud physics, may induce the intermodel diversity in cloud feedback. For example, the diversity in the strength of convective mixing between the lower and middle troposphere in models can contribute to the uncertainty in cloud feedback because of its control on low cloud fraction (Sherwood et al. 2014). Depending on the strength of deepening ABL, the entrainment rate of dry and warm air can differ, and the resultant variation in RH can cause a distinct temperature change by regulating cloud fraction even with similar changes in ET. The spread in continental warming may also arise from the different cloud physics between models; this can lead to diverse cloud responses even with similar changes in ET and RH. Thus, models with a larger cloud reduction show stronger surface warming, and this temperature rise decreases RH, thus reinforcing the positive feedback and intensifying the intermodel diversity in cloud feedback (supplemental Fig. 6). Although the causality cannot be clarified, these results imply that the magnitude of the positive cloud feedback loop can vary depending on the ET response, the strength of land–atmosphere interaction, and cloud representation in models, consequently causing intermodel spread in continental warming.

4. Summary and discussion

In this study, we examined the continental warming response to physiological forcing and quantified the resultant

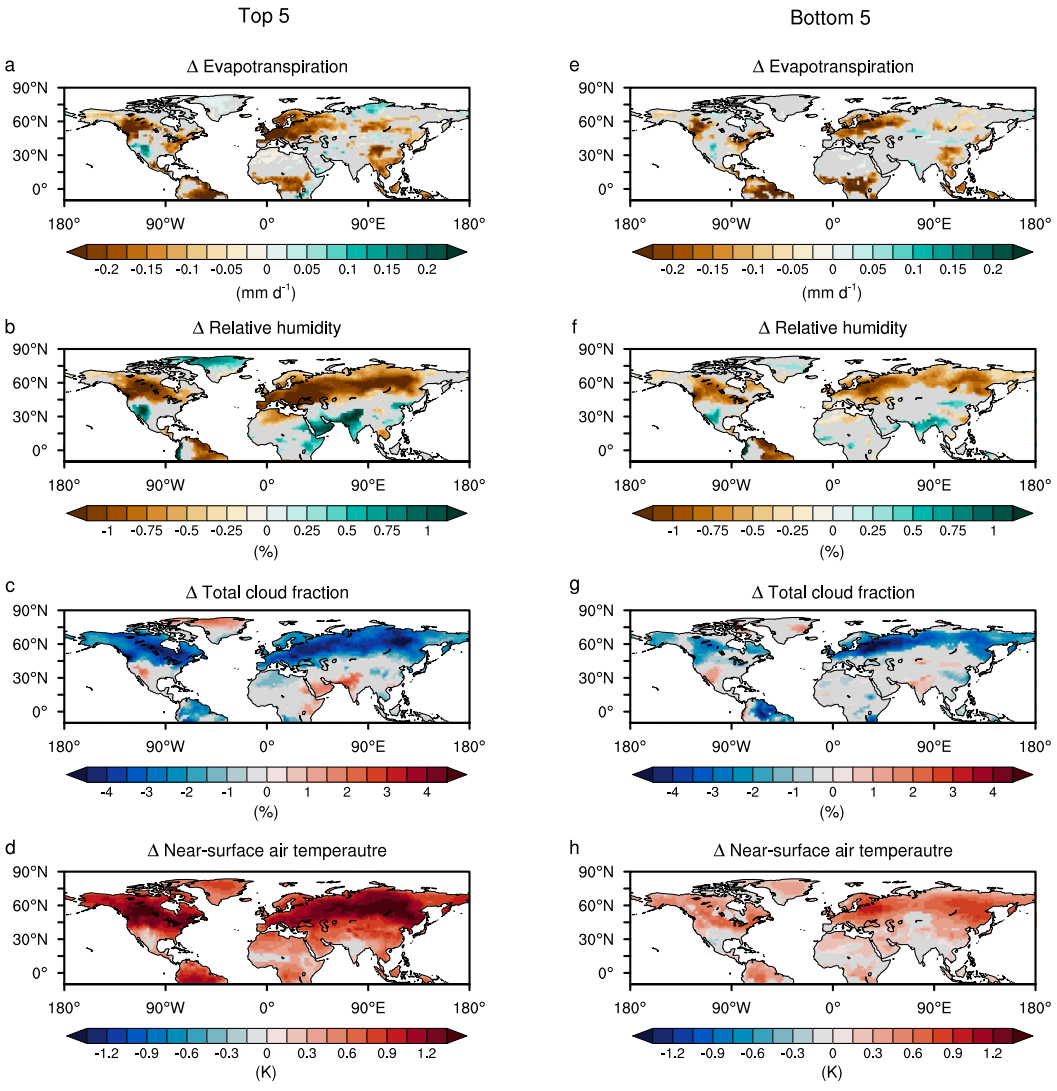

FIG. 9. Composite maps of changes resulting from CO_2 physiological forcing in (a),(e) ET, (b),(f) RH, (c),(g) total cloud fraction, and (d),(h) near-surface air temperature for (left) the top five models and (right) the bottom five models in JJA. The significant test is done based on the bootstrap method to test the model agreement. Insignificant values at the 95% confidence level are colored in gray.

climate feedback, with a focus on identifying the cause of their intermodel spread. Physiological forcing causes significant land surface warming, especially in 40°–70°N, and its intermodel diversity is considerable, which ranges from −0.24 to 1.82 K in JJA. By quantifying the temperature change associated with individual feedbacks, we demonstrated that the land surface warming response to physiological forcing is amplified primarily due to SW cloud feedback. In addition, cloud feedback plays a crucial role in the intermodel diversity of continental warming caused by the CO_2 physiological effect. Physiology explains about 13.6% of the standard deviation in mean land warming across models at 2 × CO_2 in CMIP6 (Zarakas et al. 2020); therefore, it nonnegligibly contributes to the total-CO_2-forced warming and its uncertainty. Thus, our results are expected to provide better insights into the total-CO_2-forced climate change and its uncertainty.

As mentioned above, the MME mean of the physiological-forcing-driven temperature change on land (40°–70°N) is lower in CMIP6 (annual mean: 0.5 K; σ: 0.32 K) than in CMIP5 (annual mean: 0.63 K; σ: 0.42 K). This result can be attributed to the general decrease in the magnitude of individual feedback in CMIP6 (Fig. 5). In addition, this result is due to a reflection of the tendency of a few ESMs that show feeble or even opposed physiological responses from CMIP6 (Fig. 3). In contrast to the physiological forcing, the MME mean continental warming (40°–70°N) in the CMIP6 radiative forcing experiment (annual mean: 5.08 K) is higher than that in CMIP5 (annual mean: 4.37 K) because of the overall increased warming contribution of positive feedback in CMIP6. In particular, the

cloud feedback is the largest increasing term among the individual feedback processes. This result is consistent with a previous study reporting that the global climate sensitivity produced by global climate models has an increase in CMIP6, primarily due to the strong positive cloud feedback (Zelinka et al. 2020). A further study is needed to understand how the feedback processes differently behave between the physiological and radiative forcing experiments.

In the present study, the classical forcing–feedback framework was applied for physiological and radiative forcing experiments, but a comprehensive evaluation of total-CO_2-forced climate change was not conducted. Since there is no standard definition and methodology for applying this paradigm to total-CO_2-forced climate warming, including both physiological and radiative forcings, diagnoses and their interpretation may differ depending on the definition in each study, thus complicating the comparison between studies. Doutriaux-Boucher et al. (2009) showed that stomatal closure increases radiative forcing via a rapid reduction in low clouds. Zarakas et al. (2020) suggested that this physiological effect could be included in effective radiative forcing. These studies imply that physiological responses and the resultant atmospheric adjustment can be regarded as a forcing. However, missing parts remain; in-depth studies are needed to develop an improved standard and methodology for a comprehensive radiative forcing–feedback framework considering physiological effects.

It has been suggested that the intermodel diversity in physiological forcing may come from plants' response to increasing CO_2 and atmospheric adjustment to this perturbation (Friedlingstein et al. 2006; Andrews et al. 2009; Arora et al. 2013, 2020; Piao et al. 2013; Lian et al. 2018; Devaraju et al. 2018). Our results confirm this previous finding, especially underscoring the important role of cloud feedback besides the stomatal effect in the intermodel diversity of physiological forcing. Likewise, systematic biases and weaknesses of land surface models, such as unrealistic simulations of LAI and albedo dynamics (Anav et al. 2013; Murray-Tortarolo et al. 2013; Brovkin et al. 2013) may also be contributing to this intermodel diversity and increasing the uncertainties in climate change projection. In particular, the differences in the simulated LAI and plant functional types between models may be causing the variations in vegetation forcing and plant response to CO_2 and the resultant climate feedback. These discrepancies can be a fundamental cause of intermodel diversity; thus, further research is needed on this. In addition, these issues point to the need for an improvement in the terrestrial processes embedded in ESMs based on a fundamental understanding of the involved processes. Moreover, in light of our results, physical schemes should also be improved to reduce uncertainties in simulating climate change from not only radiative forcing but also physiological forcing and thus total CO_2 forcing.

Acknowledgments. We acknowledge the World Climate Research Programme's Working Group on Coupled Modelling, which is responsible for CMIP, the climate modelling groups (listed in Table 2) for producing and making their model output, and the ESGF for archiving the data and providing access. All CMIP data are available from the ESGF repository at https://esgf-node.llnl.gov/projects/esgf-llnl/. S.-W. Park and J.-S. Kug were supported by the R&D Program for Oceans and Polar Regions of the National Research Foundation (NRF) funded by the Ministry of Science and ICT (2020M1A5A1110670). S.-Y. Jun was supported by the Earth System Model–based Korea Polar Prediction System (KPOPS-Earth) Development and Its Application to the High-Impact Weather Events originated from the Changing Arctic Ocean and Sea Ice (PE21010). J.-S. Kim was supported by the University of Zurich Research Priority Programme on Global Change and Biodiversity (URPP GCB).

REFERENCES

Ainsworth, E. A., and S. P. Long, 2005: What have we learned from 15 years of free-air CO_2 enrichment (FACE)? A meta-analytic review of the responses of photosynthesis, canopy properties and plant production to rising CO_2. *New Phytol.*, **165**, 351–372, https://doi.org/10.1111/j.1469-8137.2004.01224.x.

Anav, A., G. Murray-Tortarolo, P. Friedlingstein, S. Sitch, S. Piao, and Z. Zhu, 2013: Evaluation of land surface models in reproducing satellite derived leaf area index over the high-latitude Northern Hemisphere. Part II: Earth system models. *Remote Sens.*, **5**, 3637–3661, https://doi.org/10.3390/rs5083637.

Andrews, T., P. M. Forster, and J. M. Gregory, 2009: A surface energy perspective on climate change. *J. Climate*, **22**, 2557–2570, https://doi.org/10.1175/2008JCLI2759.1.

——, M. Doutriaux-Boucher, O. Boucher, and P. M. Forster, 2011: A regional and global analysis of carbon dioxide physiological forcing and its impact on climate. *Climate Dyn.*, **36**, 783–792, https://doi.org/10.1007/s00382-010-0742-1.

——, M. A. Ringer, M. Doutriaux-Boucher, M. J. Webb, and W. J. Collins, 2012: Sensitivity of an Earth system climate model to idealized radiative forcing. *Geophys. Res. Lett.*, **39**, L10702, https://doi.org/10.1029/2012GL051942.

Armour, K. C., C. M. Bitz, and G. H. Roe, 2013: Time-varying climate sensitivity from regional feedbacks. *J. Climate*, **26**, 4518–4534, https://doi.org/10.1175/JCLI-D-12-00544.1.

Arora, V. K., and Coauthors, 2011: Carbon emission limits required to satisfy future representative concentration pathways of greenhouse gases. *Geophys. Res. Lett.*, **38**, L05805, https://doi.org/10.1029/2010GL046270.

——, and Coauthors, 2013: Carbon–concentration and carbon–climate feedbacks in CMIP5 Earth system models. *J. Climate*, **26**, 5289–5314, https://doi.org/10.1175/JCLI-D-12-00494.1.

——, and Coauthors, 2020: Carbon–concentration and carbon–climate feedbacks in CMIP6 models and their comparison to CMIP5 models. *Biogeosciences*, **17**, 4173–4222, https://doi.org/10.5194/bg-17-4173-2020.

Bala, G., K. Caldeira, A. Mirin, M. Wickett, C. Delire, and T. J. Phillips, 2006: Biogeophysical effects of CO_2 fertilization on global climate. *Tellus*, **58B**, 620–627, https://doi.org/10.1111/j.1600-0889.2006.00210.x.

Bathiany, S., M. Claussen, and V. Brovkin, 2014: CO_2-induced Sahel greening in three CMIP5 Earth system models. *J. Climate*, **27**, 7163–7184, https://doi.org/10.1175/JCLI-D-13-00528.1.

Betts, R. A., 2000: Offset of the potential carbon sink from boreal forestation by decreases in surface albedo. *Nature*, **408**, 187–190, https://doi.org/10.1038/35041545.

——, P. M. Cox, S. E. Lee, and F. I. Woodward, 1997: Contrasting physiological and structural vegetation feedbacks in climate change simulations. *Nature*, **387**, 796–799, https://doi.org/10.1038/42924.

——, ——, M. Collins, P. P. Harris, C. Huntingford, and C. D. Jones, 2004: The role of ecosystem–atmosphere interactions in simulated Amazonian precipitation decrease and forest dieback under global climate warming. *Theor. Appl. Climatol.*, **78**, 157–175, https://doi.org/10.1007/s00704-004-0050-y.

Bony, S., and Coauthors, 2006: How well do we understand and evaluate climate change feedback processes? *J. Climate*, **19**, 3445–3482, https://doi.org/10.1175/JCLI3819.1.

Boucher, O., A. Jones, and R. A. Betts, 2009: Climate response to the physiological impact of carbon dioxide on plants in the Met Office Unified Model HadCM3. *Climate Dyn.*, **32**, 237–249, https://doi.org/10.1007/s00382-008-0459-6.

——, and Coauthors, 2020: Presentation and evaluation of the IPSL-CM6A-LR climate model. *J. Adv. Model. Earth Syst.*, **12**, e2019MS002010, https://doi.org/10.1029/2019MS002010.

Brovkin, V., L. Boysen, T. Raddatz, V. Gayler, A. Loew, and M. Claussen, 2013: Evaluation of vegetation cover and land-surface albedo in MPI-ESM CMIP5 simulations. *J. Adv. Model. Earth Syst.*, **5**, 48–57, https://doi.org/10.1029/2012MS000169.

Cao, L., G. Bala, K. Caldeira, R. Nemani, and G. Ban-Weiss, 2010: Importance of carbon dioxide physiological forcing to future climate change. *Proc. Natl. Acad. Sci. USA*, **107**, 9513–9518, https://doi.org/10.1073/pnas.0913000107.

Cess, R. D., 1990: Intercomparison and interpretation of climate feedback processes in 19 atmospheric general circulation models. *J. Geophys. Res.*, **95**, 16 601–16 615, https://doi.org/10.1029/JD095iD10p16601.

Cherchi, A., and Coauthors, 2019: Global mean climate and main patterns of variability in the CMCC-CM2 coupled model. *J. Adv. Model. Earth Syst.*, **11**, 185–209, https://doi.org/10.1029/2018MS001369.

Colman, R., 2003: A comparison of climate feedbacks in general circulation models. *Climate Dyn.*, **20**, 865–873, https://doi.org/10.1007/s00382-003-0310-z.

Cox, P. M., R. A. Betts, C. B. Bunton, R. L. H. Essery, P. R. Rowntree, and J. Smith, 1999: The impact of new land surface physics on the GCM simulation of climate and climate sensitivity. *Climate Dyn.*, **15**, 183–203, https://doi.org/10.1007/s003820050276.

Cubasch, U., and R. D. Cess, 1990: Processes and modeling. *Climate Change: The IPCC Scientific Assessment*, J. T. Houghton et al., Eds., Cambridge University Press, 69–72.

Danabasoglu, G., and Coauthors, 2020: The Community Earth System Model version 2 (CESM2). *J. Adv. Model. Earth Syst.*, **12**, e2019MS001916, https://doi.org/10.1029/2019MS001916.

de Arellano, J. V.-G., C. C. van Heerwaarden, and J. Lelieveld, 2012: Modelled suppression of boundary-layer clouds by plants in a CO_2-rich atmosphere. *Nat. Geosci.*, **5**, 701–704, https://doi.org/10.1038/ngeo1554.

Devaraju, N., N. de Noblet-Ducoudré, B. Quesada, and G. Bala, 2018: Quantifying the relative importance of direct and indirect biophysical effects of deforestation on surface temperature and teleconnections. *J. Climate*, **31**, 3811–3829, https://doi.org/10.1175/JCLI-D-17-0563.1.

Donohue, R. J., M. L. Roderick, T. R. McVicar, and G. D. Farquhar, 2013: Impact of CO_2 fertilization on maximum foliage cover across the globe's warm, arid environments. *Geophys. Res. Lett.*, **40**, 3031–3035, https://doi.org/10.1002/grl.50563.

Doutriaux-Boucher, M., M. J. Webb, J. M. Gregory, and O. Boucher, 2009: Carbon dioxide induced stomatal closure increases radiative forcing via a rapid reduction in low cloud. *Geophys. Res. Lett.*, **36**, L02703, https://doi.org/10.1029/2008GL036273.

Drake, B. G., M. A. Gonzàlez-Meler, and S. P. Long, 1997: More efficient plants: A consequence of rising atmospheric CO_2? *Annu. Rev. Plant Physiol. Plant Mol. Biol.*, **48**, 609–639, https://doi.org/10.1146/annurev.arplant.48.1.609.

Dufresne, J.-L., and Coauthors, 2013: Climate change projections using the IPSL-CM5 Earth system model: From CMIP3 to CMIP5. *Climate Dyn.*, **40**, 2123–2165, https://doi.org/10.1007/s00382-012-1636-1.

Dunne, J. P., and Coauthors, 2012: GFDL's ESM2 global coupled climate–carbon Earth system models. Part I: Physical formulation and baseline simulation characteristics. *J. Climate*, **25**, 6646–6665, https://doi.org/10.1175/JCLI-D-11-00560.1.

Eyring, V., S. Bony, G. A. Meehl, C. A. Senior, B. Stevens, R. J. Stouffer, and K. E. Taylor, 2016: Overview of the Coupled Model Intercomparison Project Phase 6 (CMIP6) experimental design and organization. *Geosci. Model Dev.*, **9**, 1937–1958, https://doi.org/10.5194/gmd-9-1937-2016.

Fatichi, S., S. Leuzinger, A. Paschalis, J. A. Langley, A. Donnellan Barraclough, and M. J. Hovenden, 2016: Partitioning direct and indirect effects reveals the response of water-limited ecosystems to elevated CO_2. *Proc. Natl. Acad. Sci. USA*, **113**, 12 757–12 762, https://doi.org/10.1073/pnas.1605036113.

Friedlingstein, P., and Coauthors, 2006: Climate–carbon cycle feedback analysis: Results from the C^4MIP model intercomparison. *J. Climate*, **19**, 3337–3353, https://doi.org/10.1175/JCLI3800.1.

Geoffroy, O., D. Saint-Martin, and A. Ribes, 2012: Quantifying the sources of spread in climate change experiments. *Geophys. Res. Lett.*, **39**, L24703, https://doi.org/10.1029/2012GL054172.

Giorgetta, M. A., and Coauthors, 2013: Climate and carbon cycle changes from 1850 to 2100 in MPI-ESM simulations for the Coupled Model Intercomparison Project phase 5. *J. Adv. Model. Earth Syst.*, **5**, 572–597, https://doi.org/10.1002/jame.20038.

Goosse, H., and Coauthors, 2018: Quantifying climate feedbacks in polar regions. *Nat. Commun.*, **9**, 1919, https://doi.org/10.1038/s41467-018-04173-0.

Gregory, J. M., and P. M. Forster, 2008: Transient climate response estimated from radiative forcing and observed temperature change. *J. Geophys. Res.*, **113**, D23105, https://doi.org/10.1029/2008JD010405.

——, and Coauthors, 2004: A new method for diagnosing radiative forcing and climate sensitivity. *Geophys. Res. Lett.*, **31**, L03205, https://doi.org/10.1029/2003GL018747.

——, T. Andrews, and P. Good, 2015: The inconstancy of the transient climate response parameter under increasing CO_2. *Philos. Trans. Roy. Soc.*, **373A**, 20140417, https://doi.org/10.1098/rsta.2014.0417.

Gunderson, C. A., and S. D. Wullschleger, 1994: Photosynthetic acclimation in trees to rising atmospheric CO_2: A broader perspective. *Photosynth. Res.*, **39**, 369–388, https://doi.org/10.1007/BF00014592.

Hajima, T., and Coauthors, 2020: Development of the MIROC-ES2L Earth system model and the evaluation of biogeochemical processes and feedbacks. *Geosci. Model Dev.*, **13**, 2197–2244, https://doi.org/10.5194/gmd-13-2197-2020.

Hansen, J., A. Lacis, D. Rind, G. Russell, P. Stone, I. Fung, R. Ruedy, and J. Lerner, 1984: Climate sensitivity: Analysis of feedback mechanisms. *Climate Processes and Climate Sensitivity*, *Geophys. Monogr.*, Vol. 29, Amer. Geophys. Union, 130–163, https://doi.org/10.1029/GM029p0130.

Hong, T., W. Dong, D. Ji, T. Dai, S. Yang, and T. Wei, 2019: The response of vegetation to rising CO_2 concentrations plays an important role in future changes in the hydrological cycle.

Theor. Appl. Climatol., **136**, 135–144, https://doi.org/10.1007/s00704-018-2476-7.

Hwang, J., Y.-S. Choi, W. Kim, H. Su, and J. H. Jiang, 2018: Observational estimation of radiative feedback to surface air temperature over northern high latitudes. *Climate Dyn.*, **50**, 615–628, https://doi.org/10.1007/s00382-017-3629-6.

Hwang, Y.-T., D. M. W. Frierson, and J. E. Kay, 2011: Coupling between Arctic feedbacks and changes in poleward energy transport. *Geophys. Res. Lett.*, **38**, L17704, https://doi.org/10.1029/2011GL048546.

Jones, C. D., and Coauthors, 2011: The HadGEM2-ES implementation of CMIP5 centennial simulations. *Geosci. Model Dev.*, **4**, 543–570, https://doi.org/10.5194/gmd-4-543-2011.

——, and Coauthors, 2016: C4MIP—The Coupled Climate–Carbon Cycle Model Intercomparison Project: Experimental protocol for CMIP6. *Geosci. Model Dev.*, **9**, 2853–2880, https://doi.org/10.5194/gmd-9-2853-2016.

Joshi, M. M., J. M. Gregory, M. J. Webb, D. M. H. Sexton, and T. C. Johns, 2008: Mechanisms for the land/sea warming contrast exhibited by simulations of climate change. *Climate Dyn.*, **30**, 455–465, https://doi.org/10.1007/s00382-007-0306-1.

Keenan, T. F., D. Y. Hollinger, G. Bohrer, D. Dragoni, J. W. Munger, H. P. Schmid, and A. D. Richardson, 2013: Increase in forest water-use efficiency as atmospheric carbon dioxide concentrations rise. *Nature*, **499**, 324–327, https://doi.org/10.1038/nature12291.

Kergoat, L., S. Lafont, H. Douville, B. Berthelot, G. Dedieu, S. Planton, and J.-F. Royer, 2002: Impact of doubled CO_2 on global-scale leaf area index and evapotranspiration: Conflicting stomatal conductance and LAI responses. *J. Geophys. Res.*, **107**, 4808, https://doi.org/10.1029/2001JD001245.

Knutti, R., and G. C. Hegerl, 2008: The equilibrium sensitivity of the Earth's temperature to radiation changes. *Nat. Geosci.*, **1**, 735–743, https://doi.org/10.1038/ngeo337.

Lammertsma, E. I., H. J. de Boer, S. C. Dekker, D. L. Dilcher, A. F. Lotter, and F. Wagner-Cremer, 2011: Global CO_2 rise leads to reduced maximum stomatal conductance in Florida vegetation. *Proc. Natl. Acad. Sci. USA*, **108**, 4035–4040, https://doi.org/10.1073/pnas.1100371108.

Lemordant, L., P. Gentine, A. S. Swann, B. I. Cook, and J. Scheff, 2018: Critical impact of vegetation physiology on the continental hydrologic cycle in response to increasing CO_2. *Proc. Natl. Acad. Sci. USA*, **115**, 4093–4098, https://doi.org/10.1073/pnas.1720712115.

Lian, X., and Coauthors, 2018: Partitioning global land evapotranspiration using CMIP5 models constrained by observations. *Nat. Climate Change*, **8**, 640–646, https://doi.org/10.1038/s41558-018-0207-9.

Lindsay, K., and Coauthors, 2014: Preindustrial-control and twentieth-century carbon cycle experiments with the Earth system model CESM1(BGC). *J. Climate*, **27**, 8981–9005, https://doi.org/10.1175/JCLI-D-12-00565.1.

Long, S. P., E. A. Ainsworth, A. D. B. Leakey, J. Nösberger, and D. R. Ort, 2006: Food for thought: Lower-than-expected crop yield stimulation with rising CO_2 concentrations. *Science*, **312**, 1918–1921, https://doi.org/10.1126/science.1114722.

Mauritsen, T., and Coauthors, 2019: Developments in the MPI-M Earth System Model version 1.2 (MPI-ESM1.2) and its response to increasing CO_2. *J. Adv. Model. Earth Syst.*, **11**, 998–1038, https://doi.org/10.1029/2018MS001400.

Medlyn, B. E., and Coauthors, 2001: Stomatal conductance of forest species after long-term exposure to elevated CO_2 concentration: A synthesis. *New Phytol.*, **149**, 247–264, https://doi.org/10.1046/j.1469-8137.2001.00028.x.

Murray-Tortarolo, G., and Coauthors, 2013: Evaluation of land surface models in reproducing satellite-derived LAI over the high-latitude Northern Hemisphere. Part I: Uncoupled DGVMs. *Remote Sens.*, **5**, 4819–4838, https://doi.org/10.3390/rs5104819.

Park, S.-W., J.-S. Kim, and J.-S. Kug, 2020: The intensification of Arctic warming as a result of CO_2 physiological forcing. *Nat. Commun.*, **11**, 2098, https://doi.org/10.1038/s41467-020-15924-3.

Pearson, R. G., S. J. Phillips, M. M. Loranty, P. S. A. Beck, T. Damoulas, S. J. Knight, and S. J. Goetz, 2013: Shifts in Arctic vegetation and associated feedbacks under climate change. *Nat. Climate Change*, **3**, 673–677, https://doi.org/10.1038/nclimate1858.

Piao, S., and Coauthors, 2013: Evaluation of terrestrial carbon cycle models for their response to climate variability and to CO_2 trends. *Global Change Biol.*, **19**, 2117–2132, https://doi.org/10.1111/gcb.12187.

Pithan, F., and T. Mauritsen, 2014: Arctic amplification dominated by temperature feedbacks in contemporary climate models. *Nat. Geosci.*, **7**, 181–184, https://doi.org/10.1038/ngeo2071.

Roe, G., 2009: Feedbacks, timescales, and seeing red. *Annu. Rev. Earth Planet. Sci.*, **37**, 93–115, https://doi.org/10.1146/annurev.earth.061008.134734.

——, N. Feldl, K. C. Armour, Y.-T. Hwang, and D. M. W. Frierson, 2015: The remote impacts of climate feedbacks on regional climate predictability. *Nat. Geosci.*, **8**, 135–139, https://doi.org/10.1038/ngeo2346.

Rose, B. E. J., K. C. Armour, D. S. Battisti, N. Feldl, and D. D. B. Koll, 2014: The dependence of transient climate sensitivity and radiative feedbacks on the spatial pattern of ocean heat uptake. *Geophys. Res. Lett.*, **41**, 1071–1078, https://doi.org/10.1002/2013GL058955.

Schimel, D., B. B. Stephens, and J. B. Fisher, 2015: Effect of increasing CO_2 on the terrestrial carbon cycle. *Proc. Natl. Acad. Sci. USA*, **112**, 436–441, https://doi.org/10.1073/pnas.1407302112.

Séférian, R., and Coauthors, 2019: Evaluation of CNRM Earth System Model, CNRM-ESM2-1: Role of Earth system processes in present-day and future climate. *J. Adv. Model. Earth Syst.*, **11**, 4182–4227, https://doi.org/10.1029/2019MS001791.

Seland, Ø., and Coauthors, 2020: Overview of the Norwegian Earth System Model (NorESM2) and key climate response of CMIP6 DECK, historical, and scenario simulations. *Geosci. Model Dev.*, **13**, 6165–6200, https://doi.org/10.5194/gmd-13-6165-2020.

Sellar, A. A., and Coauthors, 2019: UKESM1: Description and evaluation of the U.K. Earth System Model. *J. Adv. Model. Earth Syst.*, **11**, 4513–4558, https://doi.org/10.1029/2019MS001739.

Sellers, P. J., and Coauthors, 1996: Comparison of radiative and physiological effects of doubled atmospheric CO_2 on climate. *Science*, **271**, 1402–1406, https://doi.org/10.1126/science.271.5254.1402.

Shell, K. M., J. T. Kiehl, and C. A. Shields, 2008: Using the radiative kernel technique to calculate climate feedbacks in NCAR's Community Atmospheric Model. *J. Climate*, **21**, 2269–2282, https://doi.org/10.1175/2007JCLI2044.1.

Sherwood, S. C., S. Bony, and J.-L. Dufresne, 2014: Spread in model climate sensitivity traced to atmospheric convective mixing. *Nature*, **505**, 37–42, https://doi.org/10.1038/nature12829.

Skinner, C. B., C. J. Poulsen, R. Chadwick, N. S. Diffenbaugh, and R. P. Fiorella, 2017: The role of plant CO_2 physiological forcing in shaping future daily-scale precipitation. *J. Climate*, **30**, 2319–2340, https://doi.org/10.1175/JCLI-D-16-0603.1.

——, ——, and J. S. Mankin, 2018: Amplification of heat extremes by plant CO_2 physiological forcing. *Nat. Commun.*, **9**, 1094, https://doi.org/10.1038/s41467-018-03472-w.

Soden, B. J., and I. M. Held, 2006: An assessment of climate feedbacks in coupled ocean–atmosphere models. *J. Climate*, **19**, 3354–3360, https://doi.org/10.1175/JCLI3799.1.

——, ——, R. Colman, K. M. Shell, J. T. Kiehl, and C. A. Shields, 2008: Quantifying climate feedbacks using radiative kernels. *J. Climate*, **21**, 3504–3520, https://doi.org/10.1175/2007JCLI2110.1.

Stuecker, M. F., and Coauthors, 2018: Polar amplification dominated by local forcing and feedbacks. *Nat. Climate Change*, **8**, 1076–1081, https://doi.org/10.1038/s41558-018-0339-y.

Swann, A. L. S., F. M. Hoffman, C. D. Koven, and J. T. Randerson, 2016: Plant responses to increasing CO_2 reduce estimates of climate impacts on drought severity. *Proc. Natl. Acad. Sci. USA*, **113**, 10 019–10 024, https://doi.org/10.1073/pnas.1604581113.

Swart, N. C., and Coauthors, 2019: The Canadian Earth System Model version 5 (CanESM5.0.3). *Geosci. Model Dev.*, **12**, 4823–4873, https://doi.org/10.5194/gmd-12-4823-2019.

Taylor, K. E., R. J. Stouffer, and G. A. Meehl, 2012: An overview of CMIP5 and the experiment design. *Bull. Amer. Meteor. Soc.*, **93**, 485–498, https://doi.org/10.1175/BAMS-D-11-00094.1.

Tjiputra, J. F., C. Roelandt, M. Bentsen, D. M. Lawrence, T. Lorentzen, J. Schwinger, Ø. Seland, and C. Heinze, 2013: Evaluation of the carbon cycle components in the Norwegian Earth System Model (NorESM). *Geosci. Model Dev.*, **6**, 301–325, https://doi.org/10.5194/gmd-6-301-2013.

Winton, M., K. Takahashi, and I. M. Held, 2010: Importance of ocean heat uptake efficacy to transient climate change. *J. Climate*, **23**, 2333–2344, https://doi.org/10.1175/2009JCLI3139.1.

Wu, T., and Coauthors, 2013: Global carbon budgets simulated by the Beijing Climate Center Climate System Model for the last century. *J. Geophys. Res. Atmos.*, **118**, 4326–4347, https://doi.org/10.1002/jgrd.50320.

——, and Coauthors, 2019: The Beijing Climate Center Climate System Model (BCC-CSM): The main progress from CMIP5 to CMIP6. *Geosci. Model Dev.*, **12**, 1573–1600, https://doi.org/10.5194/gmd-12-1573-2019.

Yoshimori, M., M. Watanabe, H. Shiogama, A. Oka, A. Abe-Ouchi, R. Ohgaito, and Y. Kamae, 2016: A review of progress towards understanding the transient global mean surface temperature response to radiative perturbation. *Prog. Earth Planet. Sci.*, **3**, 21, https://doi.org/10.1186/s40645-016-0096-3.

Zarakas, C. M., A. L. S. Swann, M. M. Laguë, K. C. Armour, and J. T. Randerson, 2020: Plant physiology increases the magnitude and spread of the transient climate response to CO_2 in CMIP6 Earth system models. *J. Climate*, **33**, 8561–8578, https://doi.org/10.1175/JCLI-D-20-0078.1.

Zelinka, M. D., T. A. Myers, D. T. McCoy, S. Po-Chedley, P. M. Caldwell, P. Ceppi, S. A. Klein, and K. E. Taylor, 2020: Causes of higher climate sensitivity in CMIP6 models. *Geophys. Res. Lett.*, **47**, e2019GL085782, https://doi.org/10.1029/2019GL085782.

Zeng, Z., and Coauthors, 2017: Climate mitigation from vegetation biophysical feedbacks during the past three decades. *Nat. Climate Change*, **7**, 432–436, https://doi.org/10.1038/nclimate3299.

Zhu, Z., and Coauthors, 2016: Greening of the Earth and its drivers. *Nat. Climate Change*, **6**, 791–795, https://doi.org/10.1038/nclimate3004.

Ziehn, T., and Coauthors, 2020: The Australian Earth system model: ACCESS-ESM1.5. *J. South. Hemisphere Earth Syst. Sci.*, **70**, 193–214, https://doi.org/10.1071/ES19035.